

This is the accepted manuscript made available via CHORUS. The article has been published as:

Stability Landscape of Shell Buckling

Emmanuel Viot, Tobias Kreilos, Tobias M. Schneider, and Shmuel M. Rubinstein

Phys. Rev. Lett. **119**, 224101 — Published 28 November 2017

DOI: [10.1103/PhysRevLett.119.224101](https://doi.org/10.1103/PhysRevLett.119.224101)

Stability landscape of shell buckling

Emmanuel Viro^{1,2}, Tobias Kreilos¹, Tobias M. Schneider¹, and Shmuel M. Rubinstein²

¹*Emergent Complexity in Physical Systems Laboratory (ECPS),*

École Polytechnique Fédérale de Lausanne, CH 1015 Lausanne, Switzerland and

²*John A. Paulson School of Engineering and Applied Sciences, Harvard University, Cambridge, MA 02138, USA*

We measure the response of cylindrical shells to poking and identify a stability landscape, which fully characterizes the stability of perfect shells and imperfect ones in the case where a single defect dominates. We show that the landscape of stability is independent of the loading protocol and the poker geometry. **Our results suggest that the complex stability of shells reduces to a low dimensional description.** Tracking ridges and valleys of this landscape defines natural phase-space coordinates for describing the stability of shells.

From soda cans to aerospace engineering, the need of high-fidelity estimates of the buckling loads of shell structures is of critical importance for reliance or to increase payload capability [1–3]. Past laboratory testings with cylindrical shells have suggested that defects strongly reduce the buckling resistance of thin-walled structures [4–6]; thus, predicting the critical buckling loads is challenging and requires *a priori* knowledge of the defect specifics. However, those defects are in general unknown and in many cases difficult to identify. An attractive question is to investigate if there is a more general framework for characterizing the stability of shells and the classification of defects. Promising paths have been recently proposed for estimating the resistance of shells to buckling by probing them *via* poking from the side [7–9]. Additionally, a new approach has recently been proposed where instead of considering the linear instability of a shell with defects, a finite, nonlinear destabilizing perturbation is imposed on an otherwise perfect shell [10]. In this framework, buckling dynamics are governed by fully nonlinear edge-states located on the border of the basin of attraction of a stable unbuckled fixed point. These strategies lay a foundation for the more general description of the stability of thin-walled structures; opening a new approach for testing, predicting and controlling the stability of shell structure. However, these concepts have never been explored experimentally.

Here we experimentally uncloak the underlying stability structure of thin cylindrical shells by analyzing the buckling of commercial aluminum cans. We investigate the response and stability of cans when subjected to finite size lateral perturbations by laterally poking them with a point probe. The force-displacement curves of the probe at different axial loads unveil a rich *landscape* in the three-dimensional phase space spanned by axial load, probe displacement and probe force. Distinct regions of stability, independent of the loading protocol and independent on the poker geometry emerge. We specifically identify a *ridge* characterizing the finite work required to

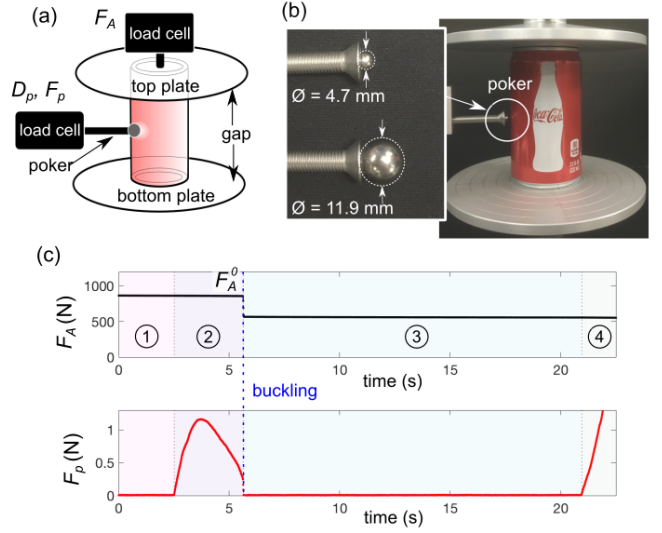


FIG. 1. **a.** Schematics of the experimental setup. **b.** The lateral poker is a steel marble glued to a screw; two different marble diameters were tested. **c.** Axial load F_A and poker force F_p for a typical experiment: (1) the shell is compressed to F_A^0 , and then the gap is fixed, (2) the poker is advanced until buckling occurs. (3) The probe catches up with the buckled shell (4).

force-trigger buckling, and we identify a *valley* leading to a minimally buckled state and representing the easiest route to buckle. We suggest that this stability landscape is archetypal to the buckling of perfect shells as well as imperfect ones; specifically in the case where one localized geometric defect dominates. Importantly, the salient topographical features are not aligned parallel to either the axial or poking force axis, indicating that more suitable coordinates for analyzing the stability of thin shells are defined by tracking ridges and valleys.

We investigate the stability of variety of real indus-

n°	fixed	varied	marble	datasets
1	axial gap	D_p	4.7 mm	89
2	axial gap	D_p (single can)	4.7 mm	5
3	axial gap	D_p	11.9 mm	14
4	axial load	D_p	4.7 mm	39
5	D_p	axial gap	4.7 mm	17

TABLE I. Protocols for the different biaxial tests.

trial cylindrical shells. A custom-made biaxial machine (ADMET, Inc.) is used to axially compress commercial aluminum cans and probe them from the side, as sketched in Fig. 1(a). The vertical axis has a resolution of $20\ \mu\text{m}$ in displacement and $0.1\ \text{N}$ force with a maximum force of $2,200\ \text{N}$. A blunt poker is installed in the horizontal axis which also has a $20\ \mu\text{m}$ displacement resolution. The poker force is measured by an S-beam load cell with $5\ \text{mN}$ resolution and a maximal load of $100\ \text{N}$. We tested many brands and geometries of commercial soda cans; however, in this letter we focus on a single size and present experiments conducted with cylindrical shells of radius $R = 28.6\ \text{mm}$, a thickness $t = 104\ \mu\text{m}$ (radius-to-thickness ratio $R/t = 274$) and a total height $L = 107\ \text{mm}$. Similar results were obtained for all brands and geometries. Two types of poker tips are used, covering a range of diameters large enough to not puncture the shell but much smaller than the shell diameter, as shown in Fig. 1(b) and tabulated in Table 1. Within this range results do not appear to depend on the geometry of the poker tip.

Shells are initially compressed at a constant speed of $1\ \text{mm/min}$ to a pre-set axial load $F_A = F_A^0$. When the pre-set load is reached, the gap is fixed and F_A is monitored while the horizontal poker is advanced towards the shell at a constant speed $10\ \text{mm/min}$. The poker force F_p is simultaneously recorded. Initially, F_p increases - *similarly to the first stages of reported shell pokings [11, 12]* - reaches a maximum, and then decreases. During this time, F_A does not change significantly. Eventually, when F_p reaches zero, the shell buckles at the point of poking and a sharp drop of F_A is observed, as shown for a typical example in Fig. 1(c). Such a buckling event is always accompanied by a sharp snapping sound. Alternative loading protocols were also tested and did not change the results. For instance, tests were performed where instead of fixing the vertical gap, the vertical load F_A was kept constant through feedback (4 in Table 1). This protocol consistently show the same typical dynamics to the *gap controlled* protocols (1 – 3, 5 in Table 1).

The shell stability is investigated by poking individual cans from the side with F_A^0 ranging from $100\ \text{N}$ to $1100\ \text{N}$. Depending on F_A^0 , testing reveals a plethora of

stereotypical responses, with three qualitatively different regimes. For axial loads *below* $400\ \text{N}$, F_p monotonically increases, as shown by the top two curves in Fig. 2(a). In this regime the shells are stable and do not buckle. A second regime emerges in the range between $400\ \text{N}$ and $700\ \text{N}$ the shells still do not buckle but $F_p(D_p)$ curves are more detailed and non-monotonic, exhibiting a maximum force, F_p^{max} , at D_p^{max} , and then a local minimum force, F_p^{min} , at D_p^{min} , as shown for $F_A = 467\ \text{N}$ and $F_A = 675\ \text{N}$ in Fig. 2(a). For $F_A > 700\ \text{N}$ poking eventually leads to buckling. $F_p(D_p)$ shows a maximum, $(D_p^{\text{max}}, F_p^{\text{max}})$, however the force curve will no longer show a minimum; instead, at a critical distance, D_p^c , the poking force vanishes, $F_p(D_p^c) = 0$, and at this point the shells becomes unstable, and buckles, as shown for $F_A^0 = 683\ \text{N}$, $F_A^0 = 859\ \text{N}$ and $F_A^0 = 1,084\ \text{N}$ in Fig. 2(a). When buckling, the point on the shells surface that was in contact with the poker accelerates towards the inside of the shell, away from the poker. It then comes to rest at a new stable equilibrium location, D_p^s , as a single Miura-like dimple [13] remains on the surface. D_p^s is probed by advancing the horizontal poker until it comes back in contact with the aluminum surface. Concomitantly with these dynamics, buckling is also indicated by the sharp decrease in F_A , as shown in the insets of Fig. 2(a).

Up to this point we have focused on several typical examples, introducing three main possible scenarios for the dynamics. Combining all measured force-displacement data for a range of axial loads, $F_p(D_p, F_A)$ reveals a well defined surface in the three-dimensional phase space (F_A, D_p, F_p) , as shown in Fig. 2(b). It is important to note that the response curves of the poker are reversible throughout the majority of the axial load and poker force ranges. Fig. 2(c) presents these ranges, showing reversibility even in the non-monotonic phases of the response. This indicates the absence of irreversible plastic deformation. The goal of this letter is to introduce and highlight the significant topographical features of this *stability landscape* and discuss their physical significance. Although, the stability of each individual shell is uniquely determined by its specific defects, we hypothesize that the stability landscape is a generic representation of the stability of cylindrical shells. The landscape is similar for different shells of identical geometry as long as – without poking – the axial load remains far enough from the threshold where the shell spontaneously buckles. We speculate that closer to the threshold for spontaneous buckling, which depends on defects, the landscape will be smoothly distorted.

Even with a side poker it is not always possible to trigger buckling. At low axial loads F_A^0 the cylindrical shell will not buckle regardless of the poking displacement and $F_p(D_p)$ monotonically increases up to large poker penetrations of several *millimeters*. Under large axial loads,

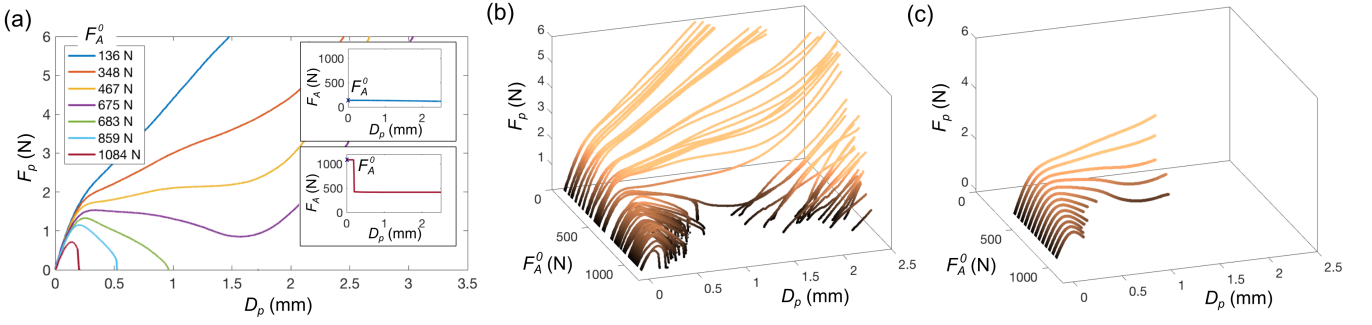


FIG. 2. **a.** Force-displacement curves for seven cans. Insets: axial load measurements. **b.** Three-dimensional representation of independent poker force measurements (1 in Table 1). The surface generated by the curves defines a landscape, which characterizes the stability of the thin shell. The color indicates F_p . **c.** Three-dimensional representation of consecutive non-destructive poker force measurements on the same can, probing reversible elastic deformations without reaching buckling (2 in Table 1).

$F_p(D_p)$ shows distinct features, indicated schematically in Fig. 3(a): the points of maximal force (D_p^{\max}, F_p^{\max}), the points of minimal force (D_p^{\min}, F_p^{\min}), and the buckling points for poker displacements ($D_p^c, F_p(D_p^c) = 0$). After buckling the dimple snaps inwards to a position ($D_p^s, 0$) [14]. D_p^{\max} decreases linearly as a function of F_A^0 , as shown in Fig. 3(b). The trajectory of the maximum F_p^{\max} is a monotonically decreasing function of F_A^0 and does not depend on the poker size (1 and 3 in Table 1), as shown in Fig. 3(c). Importantly, the stability is not altered if the compression is load-controlled instead of displacement-controlled (4 in Table 1), as shown in Fig. 3(b) and Fig. 3(c) [15]. The described characteristics of the load-displacement curves can also be obtained, with less noise, by non-destructively probing a single can at different loads (2 in Table 1), as shown in the insets of Fig. 3(b) and Fig. 3(c).

Buckling occurs for a sufficiently high axial load and beyond a critical displacement of the poker D_p^c . In all our experiments, D_p^c is at least two times larger than the shell thickness, indicating that buckling in this case is a nonlinear instability triggered by finite amplitude perturbations. The critical poker displacement D_p^c decreases linearly as a function of F_A^0 , as shown in Fig. 3(d). In a range of F_A^0 between 400 N and 600 N, D_p^c is comparable to D_p^s , indicating that buckling cannot occur below such loading. Moreover, if we first fix the position of the poker, and then increase the axial load until buckling, we find the same values of D_p^c (5 in Table 1), suggesting that the stability landscape is independent of the loading and poking history, as shown in the inset of Fig. 3(c).

In an intermediate range of axial loads centered around $F_A^0 = 600$ N, $F_p(D_p)$ has a local minimum, (D_p^{\min}, F_p^{\min}), as sketched in Fig. 3(a). Following the minima of the stability landscape down to zero poker force leads to a

minimally buckled state. Buckling does not occur for loads smaller than this minimal buckling load.

Traditionally, the linear instability of cylindrical shells against catastrophic buckling is primarily considered. At a critical axial load any infinitesimal perturbation will destabilize the system causing it to buckle. Real shells have defects and are thus weaker; it is common to only consider the linear stability of the now defected shell base state [16]. Here we are examining the stability of shells under conditions where they are linearly stable and a finite amount of work, $E_p = \int_0^{D_p^c} F_p(x) dx$, is required to destabilize them. When the axial load is larger, less work is required to collapse the shell and as the axial load approaches the critical load for the linear instability, E_p approaches zero (Fig. 3(e)) and in qualitative agreement with recent computations of the stability of pressurized spherical shells [9]. This consistency with recent computations also suggests that our concept of landscape of stability could be extended to any shell. In the linearly stable system one may think of E_p as an energy barrier to buckling that is decreased by defects.

Our results suggest that the stability of shells can be coherently described by a two-dimensional surface in the three-dimensional phase space (F_A, D_p, F_p), schematically described in Fig. 4. It is an important conclusion that the complex stability of commercial soda cans reduces to such a low dimensional description, as naively such systems should be fully dominated by stochastic defects rendering buckling thresholds unpredictable. The stability landscape presents a number of important features. The gap between the unstable fixed point D_p^c and the stable one D_p^s , shown qualitatively in Fig. 2(b), is a flat lake representing the unstable region surrounded by a basin and protected by an energy barrier, E_p . In the landscape, the energy barrier takes the form of a

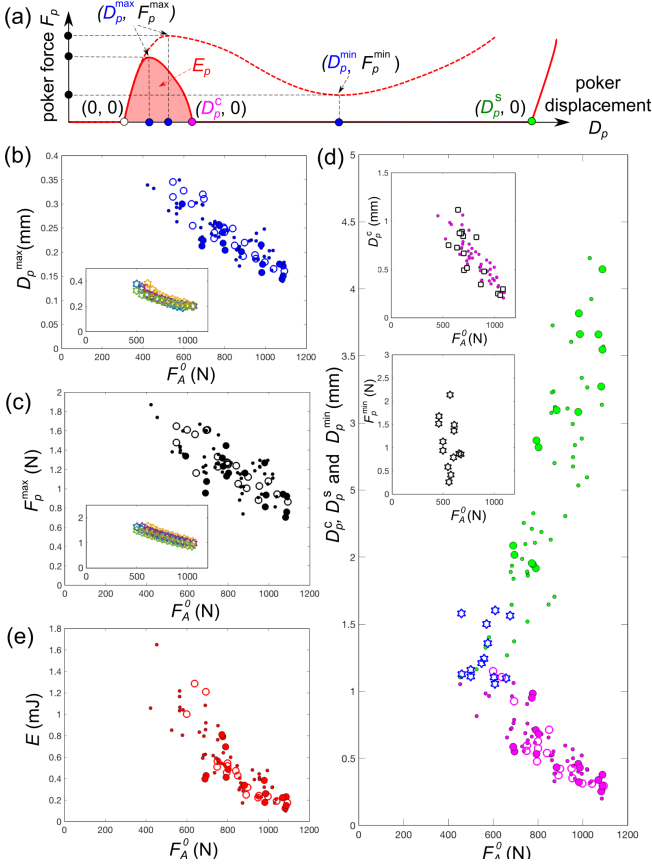


FIG. 3. All individual cans share universal stability features. **a.** Definitions of the main features. **b.** D_p^{\max} at F_p^{\max} vs F_A^0 . Small dots, large dots and circles correspond to the protocols 1, 3 and 4 respectively, indicated in Table 1. Inset: single can tests. **c.** F_p^{\max} vs F_A^0 . **d.** Critical poking displacement D_p^c required to trigger buckling (magenta) and displacement D_p^s to catch up with the post-buckled surface (green) vs F_A^0 . Inset, hollow squares: the shell is first poked and then loaded (5 in Table 1). The poking displacement D_p^{\min} at the minimum of poking force is plotted with blue stars, and the minimum poking force F_p^{\min} is reported in the second inset. **e.** The elastic energy barrier, E_p vs F_A^0 .

cliff to the left of the lake that is decorated by a ridge $R = (D_p^{\max}(F_A^0), F_p^{\max}(F_A^0))$. Although buckling may also suddenly occur in our experiments [17] by a violent drop of F_p to 0, in all our tests this never occurs for $D_p < D_p^{\max}$; thus, the ridge may indicate the separating line between a globally stable (i.e. defect-insensitive) region to the left of the ridge and a defect-sensitive region to its right. It is thus potentially useful to envision ridge-tracking as a new non-intrusive method for probing the stability of shells as close as possible to their linearly unstable limit.

Another useful feature of the stability landscape is the

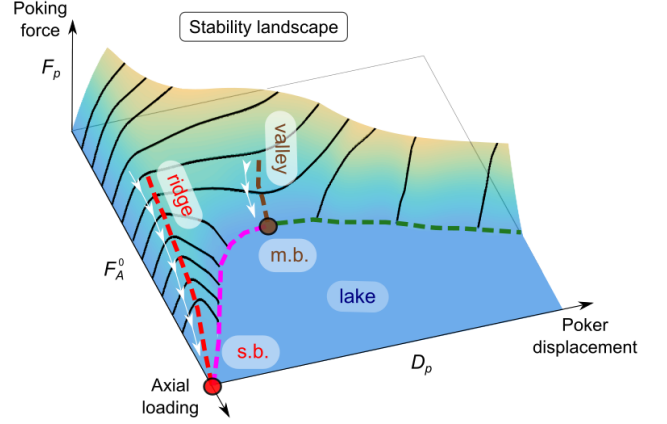


FIG. 4. A schematic demonstration of the stability landscape of shell buckling. The ridge is defined as the trajectory of the maxima of poking force $(D_p^{\max}(F_A^0), F_p^{\max}(F_A^0))$. Following the ridge down to zero poking force leads to the spontaneous buckling (s.b.). The valley is defined as the trajectory of the local force minima $(D_p^{\min}(F_A^0), F_p^{\min}(F_A^0))$. Following the valley down the zero poking force leads to a minimally buckled state (m.b.), below which no buckling is possible. The magenta and the green dashed lines corresponds to the unstable (D_p^c) and stable (D_p^s) fixed points respectively

minimal buckling point: for F_A smaller than a critical value, the shells never buckle, consistent with the phenomenological design rule set by NASA [4] and hinted to by calculations of edge states [10]. Although in this regime there is no buckling ($F_p \neq 0$), the landscape is not featureless. Instead the curve $V = (D_p^{\min}(F_A^0), F_p^{\min}(F_A^0))$ highlights a valley with a very steep slope leading to the tip of the lake where $D_p^c = D_p^s$. This tip is the point of minimal buckling, where buckling does not result in any measurable deformation of the shell.

Our results suggest an appealing and generic framework for studying the stability of thin-walled structures. Shell buckling is characterized by the topographical features of the stability landscape, namely an unstable flat lake surrounded by a basin with a ridge and valley of stability. It is tempting to consider that the ridge and valley indicate the most natural coordinate system for probing the stability of such structures instead of the somewhat arbitrary coordinates F_A^0 and D_p . Thus, systematic tracking of the ridge and the valley of the stability landscape is likely to have a significant impact in the development of new non-destructive testing protocols in structural engineering.

We have shown that buckling of real defected cylindrical shells is underscored by a universal stability landscape. By probing away from the linearly unstable state we are exposing the underlying stability characteristics of

the near-perfect shell. The probe induces a localized shell deformation; thus, illuminating how a dominant localized defect modifies the shell stability. The local geometric defect induced by the poker, interact with intrinsic defects in the shell material. Consequently, we speculate that at high axial loads a smoothly distorted stability landscape encodes the influence of localized intrinsic defects.

Here, we present the landscape for a single poker measurement revealing the influence of a dominant localized defect. Likewise, a system poked from several directions simultaneously with numerous pokers will show a different stability landscape. In fact, the full stability landscape is hyper-dimensional and any probing geometry

defines its own section of the full stability landscape; a section spanned by the amplitude of that specific probing mode, the probe force and axial load [10]. While the full stability landscape lies in the hyperspace spanned by all possible probe geometries and associated force amplitudes, it is reasonable to expect that the single localized defect case studied in this letter, is of practical importance and may inform the design rules of thin-walled structures, such as rockets, airplanes, and beer cans.

This work was supported by the NSF (DMR-1420570) and the SNSF (200021-165530, 200021-160088). SMR acknowledges support from the Alfred P. Sloan Foundation.

-
- [1] D. Bushnell, *AIAA Journal* **19** 11831226, (1981).
 - [2] R. C. Davis, F. Carder, *NASA Technical Memorandum* 88996, (1987).
 - [3] M. W. Hilburger, W. Allen Waters, W. T. Haynie, *NASA Technical Publication* TP-2015-218785, (2015).
 - [4] P. Seide, V. I. Weingarten, E. J. Morgan, *Space Technology Laboratories*, Report STL/TR- 60-0000-19425 (1960).
 - [5] W. H. Horton, S. C. Durham, *Int. J. Solids Struct.*, 5972 (1965).
 - [6] J. Singer, J. Arbocz, T. Weller, *Experimental Methods in Buckling of Thin-Walled Structures*, John Wiley & sons, New York, Volume 1 and 2 (2002).
 - [7] J. M. T. Thompson, *Int. J. Bifurcat. Chaos* **25**, 1530001 (2015).
 - [8] J. M. T. Thompson, J. Sieber, *Int. J. Bifurcat. Chaos* **26**, 1630003 (2016).
 - [9] J. W. Hutchinson, J. M. T. Thompson, *J. Appl. Mech.* **84**, 061001 (2017).
 - [10] T. Kreilos, T. M. Schneider, *P. R. Soc. Lond. A*, In Press, (2017).
 - [11] A. Pauchard, S. Rica, *Philos. Mag. B* **78**, 225-233 (1998).
 - [12] A. Boudaoud, P. Patricio, Y. Couder, M. Ben Amar, *Nature* **407**, 718-720 (2000).
 - [13] K. Miura, *New Approaches to Structural Mechanics, Shells and Biological Structures*, 329-339, (2002).
 - [14] Note that in the situations where during the buckling process several dimples are formed (more common at high axial loads), D_p^s only indicates the depth of the dimple in the direction of the poker and the other dimples are not taken into account.
 - [15] For load-controlled compression, the shell is totally crushed when buckling is induced; thus, D_p^s cannot be measured.
 - [16] A. Lee, J. Marthelot, F. Lopez Jimenez, J. W. Hutchinson, P. M. Reis, *J. Appl. Mech.* **83**, 111005 (2016).
 - [17] A violent drop in the poking force is observed for axial loads of $F_A^0 = 859$ N or $F_A^0 = 1084$ N in Fig. 2(a). In these two cases the force drops to zero significantly faster than the axial loading rate. We did not observe any rate dependence of the mechanical response in the loading rate range that we tested (0.1 to 10 mm/min).